Chapter 9

In-Silico investigation on repurposed drugs for CNS infection

Chapter 9

9. Computational biology-based investigation on repurposable drugs for CNS infection

9.1 Introduction

Acute respiratory failure and neuroinfection may result from systemic invasion caused by pulmo-neurotropic viruses, according to recent investigations. The Japanese encephalitis (JE), Severe Acute Respiratory Syndrome Coronavirus-2 (SARS-COV2), Human Immunodeficiency Virus (HIV), and Simian Immunodeficiency Virus (SIV) are just a few of the migrating neurotropic viral diseases that can be treated with the tetracycline class of secondary metabolites of microorganisms. Further, cephalosporin, a different microbial secondary metabolite, may also be employed in antiviral combination treatment. Viral resistance to such drugs, however, is a significant public health crisis; as a result, one has to investigate the antiviral potency of alternative secondary metabolites, such as phytochemicals. Therefore, in this study, we examine the therapeutic effectiveness of phytochemicals such podophyllotoxin, chlorogenic acid, naringenin, and quercetin in neurotropic viral infections.

To study the plausibility of the afferent neural route of a virus in human, MRI scanning was done on human participants, and fiber-tractography was used to analyze the connections between cranial nerves and the brain-stem/limbic-region. Furthermore, a human clinical trial evaluation ($n = 140$, $p = 0.028$) was performed in order to develop a quantitative model of antiviral pharmaceutical intervention.Furthermore, docking studies were performed to identifythe binding affinity of phytochemicals toward antiviral targets as (i) host receptor [Angiotensin-converting Enzyme-2], (ii) main protease of SARS-COV2 virus (iii) NS3-Helicase/Nucleoside triphosphatase of Japanese-encephalitis-virus, and the affinities were compared to standard tetracycline and cephalosporin antibiotics. The

potential mechanism of action of those phytochemicals was then determined using network pharmacology analysis.

The results of the human MRI-tractography investigation revealed the following fiber connections: (a) *Path-1*: From the olfactory nerve to the cerebral limbic area; (b) *Path-2*: From the peripheral glossopharyngeal nerve and vagus nerves to the midbrain-respiratory center. According to docking experiments, phytochemicals, tetracycline, and cephalosporin antibiotics have similar binding affinities for (a) viral receptors and (b) host cell receptors where virus-receptor attaches. Furthermore, the phytochemicals successfully inhibited the neuroinflammation caused by the cytokine storm, a significant pathogenic route. We also discovered that the patient survival curve under antiviral therapy is explained by a systems biology-based double-hit mathematical bi-exponential model, providing a quantitative-clinical framework of secondary metabolite action on virus and host cells.

As a consequence of the increasing viral resistance to antibiotics, we discovered new phytochemicals with clinical therapeutic potential for neurotropic virus infection. We defined the anatomical route and quantitative formulation of the mechanism of antiviral activity using human MRI scans and clinical trial findings. The clinical trial was registered with Clinical Trials Registry of India (CTRI) - CTRI/2010/091/006143.

9.2 Materials and methods

9.2.1 Image Acquisition

3T magnetic resonance scanners (Philips Achieva 3.0 Tesla at the National Neuroimaging Facility, National Brain Research Center, Manesar, India), an eight-channel head coil, and a SENSE imaging sequence were used for the scans. DTI images were obtained using an echo-planar imaging sequence with b values of 1000 s/mm2 and one reference volume with b =0 s/mm2. The DTI acquisition settings were 9386 ms repetition time, 58 ms echo time, 224x224 field of view, 2 mm slice thickness, 0 slice gap, 70 slices, and a 90° flip angle. The T1 weighted MRI volume was acquired using a turbo field echo procedure. The scanner acquisition settings were 4 ms echo time, 8.5 ms repetition time, 1x1x1 mm3 voxel size, 240x240x160 field of view, 1 mm slice thickness, 160 slices, and an 8° flip angle. Inclusion criteria were a healthy physiological state within normal limits and the absence of co-morbidities. We enrolled five healthy people in our investigation, and tractography was done on two of them at random. The Institutional Human Ethics Committee of the National Brain Research Center approved the scanning of the participants and informed consent was taken. The scans were examined by the authors, who have over 25 years of combined neuroimaging expertise.

9.2.2 Fiber Tracking with DSI Platform

The diffusion MR images are analysed by the non-profit platform DSI studio. This method is used for deterministic fiber tracing, reconstruction, and visualization in three dimensions (http://dsi-studio.labsolver.org). Using restricted diffusion imaging, the restricted diffusion was measured [168]. With a diffusion sampling length ratio of 1.25, generalized q-sampling imaging (GQI) was used to reconstruct the diffusion data [169]. A tensormetric analysis was performed. To locate fibers, a deterministic approach was used [170]. An ROI has been placed in the pons medulla to demonstrate the linkages with

gustatory nerves. Similarly, another ROI has been placed at the hippocampus, entorhinal cortex, and amygdala to demonstrate the olfactory nerve connections. A seeding area was implanted across the brain. Other settings such as the termination index quantitative anisotropy based on Otsu's threshold, the angular threshold 60 [108], the step size of 0.10 mm, the smoothing of 0, the minimum length of 5.0 mm, the maximum length of 300 mm, and the seed orientation were maintained constant while constructing all tracks [171].

9.2.3 Docking Studies

9.2.3.1 Retrieval of the Target Protein

The three-dimensional crystal structure of the SARS-COV2 spike receptor-binding domain bound to the ACE2 receptor (PDBID: 6M0J), the inhibitor bound human angiotensin-converting enzyme-related carboxypeptidase (ACE2) (PDB ID: 1R4L), the N3 inhibitor bound COVID-19 main protease (PDB ID: 6LU7), and JEV NS3 helicase/NTPase (PDB ID: 2Z83) protein were downloaded from the RCSB Protein Data Bank.

9.2.3.2 Selection of Ligands and Its Optimization

The chemical structures of podophyllotoxin, chlorogenic acid, naringenin, quercetin, and tetracycline class (Tetracycline, Minocycline, and Doxycycline) of antibiotics, the newer type of tetracycline like flurocycline (Ervacycline) and glycylcycline (Tigecycline), cephalosporin ceftriaxone, angiotensin-converting enzyme inhibitors MLN-4760, and lisinopril were obtained from the PubChem compound database in the SDF format. Using the PyRx tool, the ligands' energy was minimized before being translated to the PDB format. The ligand was once again translated into the PDBQT format for the docking investigation by incorporating charges (Q) and bond types (T).

9.2.3.3 Molecular Docking Procedure

In order to identify the specific amino acid residues involved in this interaction, the inhibitor bound with the ACE2 receptor (PDB ID: 1R4L) and the SARS-COV2 spike

receptor-binding domain (PDB ID: 6M0J) were first removed from the ACE2 receptor's active site. Similar to this, the major protease of SARS-COV2 had its N3 inhibitor removed in order to identify the interaction amino acid residues. Then, an appropriate grid box that was sufficiently big to include all of the interfering residues was constructed. The center of the grid box was set for the SARS-COV2 spike receptor-binding domain (PDB ID: 6M0J) at 32.977, 31.22, and 19.684, and the box size was set at 68, 88, and 96 in the x, y, and z directions, respectively. Similar to this, for the inhibitor bound to the ACE2 receptor (PDB ID: 1R4L), the grid box's center was placed at 39.906, 3.092, and 22.477, and the box size was set at 52, 68, and 60, correspondingly. The grid box's center and size were adjusted at 15.62, 11.684, and 66.738 in the x, y, and z axes, respectively, for the SARS-COV2 major protease (PDB ID: 6LU7). For confirmation, the original co-crystallized ligand for PDB IDs 1R4L, 6LU7, and 6M0J as well as the bound protein for PDB ID: 6M0J were superimposed. The RMSD value was then determined, and its values were discovered to be 2.042, 0.362, 2.22, and 0.066, respectively.

The Lamarckian evolutionary approach was utilized to compute the ACE2 receptor-ligand interaction in AutoDock Version 1.5.6[172]. In AutoDock, which calculates the inhibition constant (Ki) of the receptor-ligand complex, the binding affinity of the ligands for the COVID-19 binding site of the ACE2 receptor was estimated. Intermolecular energy, the total internal energy of the ligand, and torsional free energy were the three main types of binding energies produced by AutoDock. Hess' law states that the free energy of binding is equal to the sum of the intermolecular and torsional-free energies, which is subsequently transformed into an inhibition constant (Ki). The binding affinity of the ligands to the receptor was calculated using the lowest free binding energy value and its Ki value. By superimposing the macromolecule retrieved from the protein data repository with the docked protein, the RMSD of the docking process is determined.

9.2.4 Network Pharmacology

9.2.4.1 Retrieval of the Target Genes

Targets of standard drugs and phytochemicals specific to neuroinflammation were retrieved from different databases, suchas GeneCard [172], Drugbank, and literature review. Moreover, the SARS-COV2 and Japanese Encephalitis target proteins are retrieved from UniProt (https://www.uniprot.org/), GeneCard, and NCBI [173]. Furthermore, Venn diagram analysis was done to identify the common targets in COVID-19 and JE disease with individual therapeutic agents using the Venny tool.

9.2.4.2 Network Construction and Topological Analysis

Selected target genes common for an individual therapeutic agent with both the COVID-19 and JE virus target geneswere imported in Cytoscape plugin, GeneMANIA (Multiple Association Network Integration Algorithm) to construct their network based on their functional relations [174]. The resulting networks of genes were then analysed based on their co-expression, genetic interaction, physical interaction, pathway, colocalization, and predicted and shared protein domains. Furthermore, the CytoNCA plugin was used tostudy the topological parameters, such as betweenness centrality, degree centrality, and closeness centrality of the resulting network [175].

9.2.4.3 Gene Ontology (GO) and KEGG Enrichment Analysis of Targets

Gene ontology is a way to depict detailed information of genes and their products in terms of molecular function (MF), biological process (BP), and cellular component (CC)[176]. We have used the PANTHER (Protein Analysis Through Evolutionary Relationships) tool for GO analysisof selected target genes with their role in different KEGG pathways [177]. Genes predicted to be involvedin the neuroinflammatory response and neurorespiratory viral infection from GO term analysis were compared with CytoNCA

predicted genes. Furthermore, those genes were identified from the Coronavirus disease KEGG pathway (map05171) to understand their functions.

9.3 Results

9.3.1 MRI Tractography Analysis

9.3.1.1 Connection Between Brain Stem and Gustatory Nerves

Utilizing Diffusion MRI fiber tracking, the connections between brain stem (medulla oblongata and pons) where the respiratory center is located and the three gustatory nerves, which are glossopharyngeal (CNIX) that carries taste sensation from the posterior region of the mouth and the throat, facial nerve (CNVII) from the chorda tympani and the vagus nerve (CNX) from the base of the tongue and other parts of the pharyngeal region, were visualized. Besides that, the hypoglossal nerve (CNXII), which innervates the muscles of the tongue, gives tracts with pons. Using HCP1021tractography atlas, fibers passing through every two ROI pairs were identified (Figure 46, Figure 47).

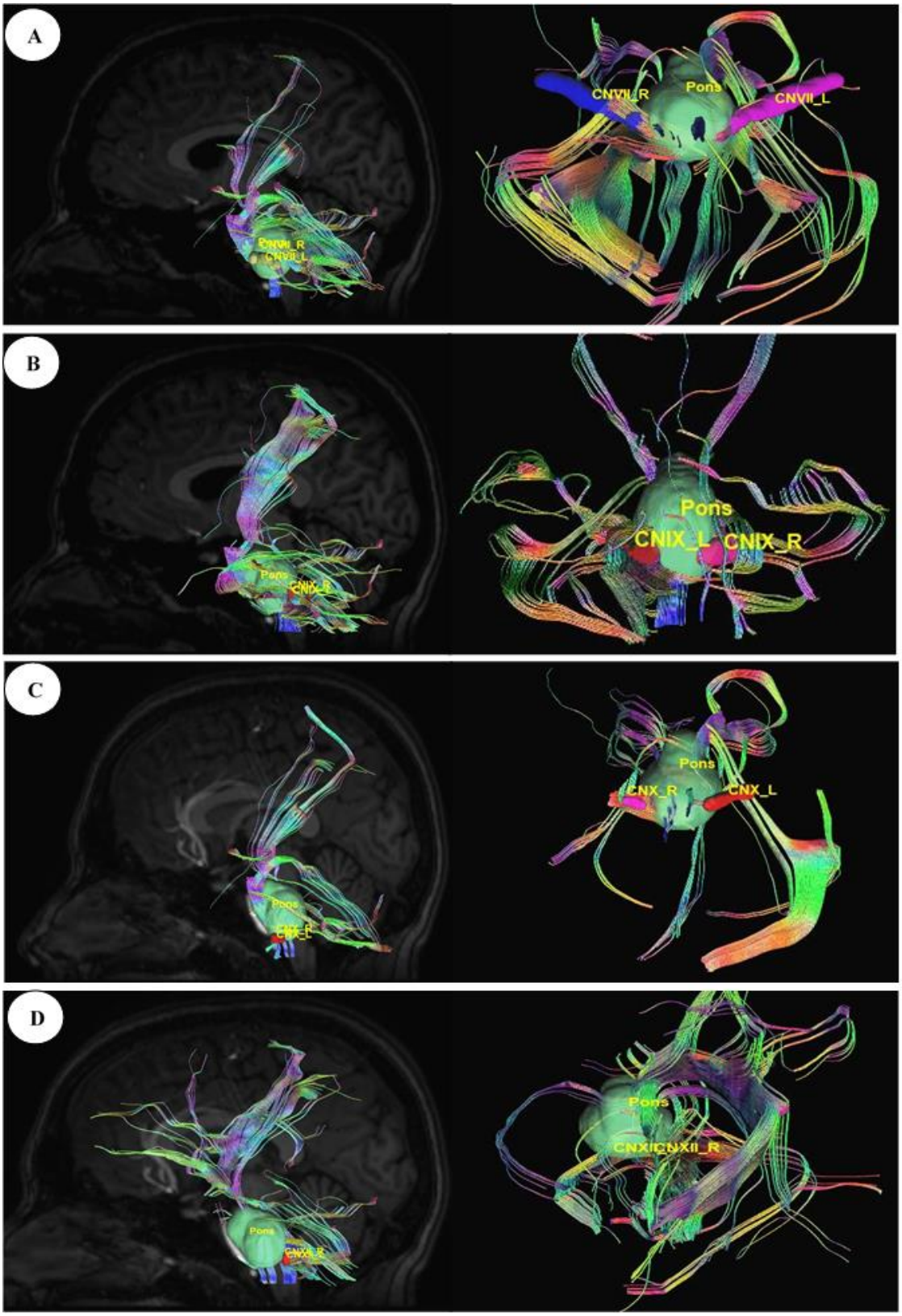

Figure 46: *Diffusion MRI fiber tracking-connecting pons with the gustatory nerves. (A) pons to cranial nerves VII, (B) pons to cranial nerves IX, (C) pons to cranialnerves X, and (D) pons to cranial nerves XII.*

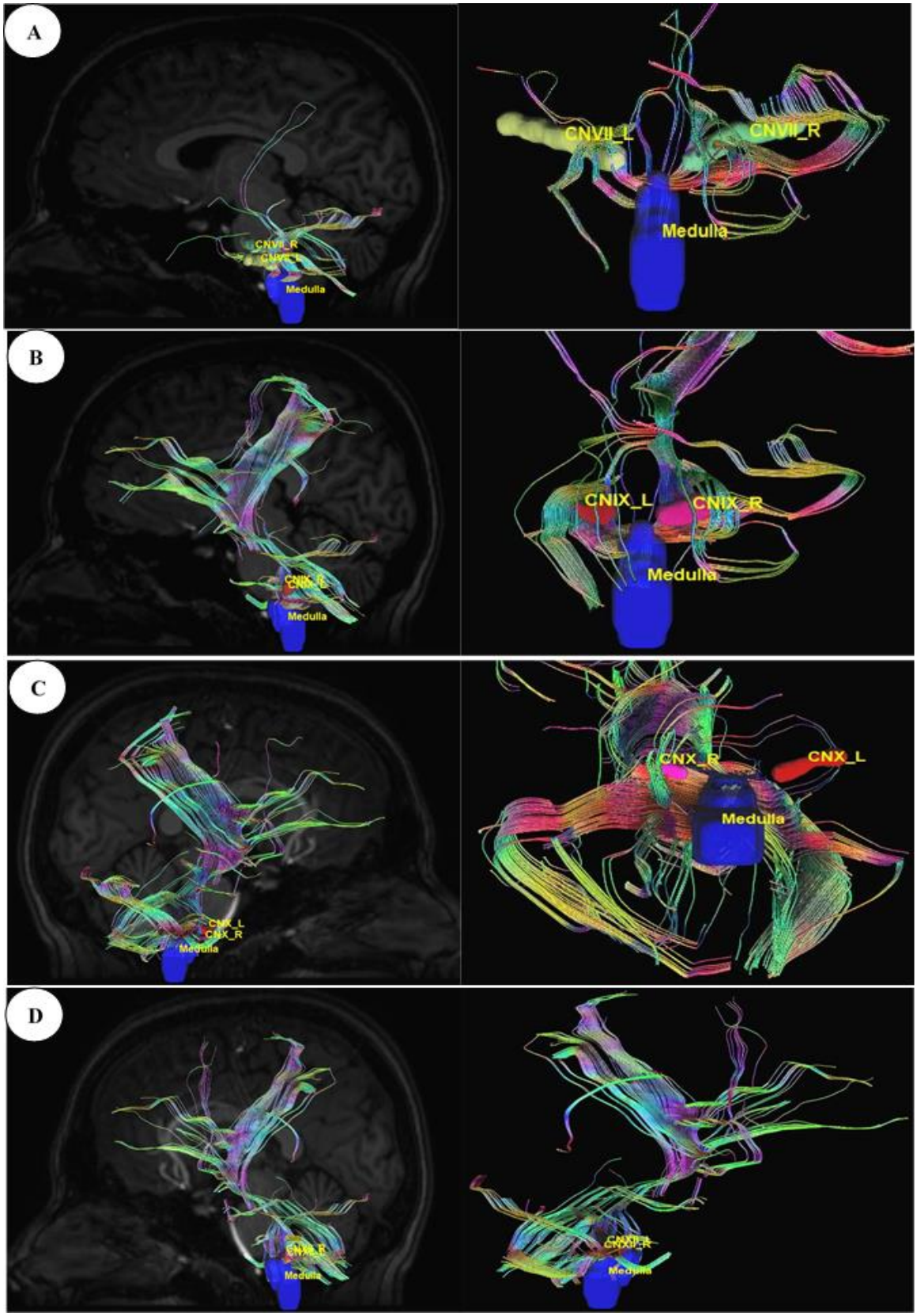

Figure 47: *Diffusion MRI fiber tracking connecting medulla oblongata with gustatory nerves. (A) medulla to cranial nerve VII, (B) medulla to cranial nerve IX, (C)medulla to cranial nerve X, and (D) medulla to cranial nerve XI.*

9.3.1.2 Connection Between Limbic System and Olfactory Nerves

The connections between the olfactory nerve, which is also known as the olfactory tract coming out from the olfactory bulb and the important area of the limbic system hippocampus, the entorhinal cortex, and the amygdala were visualized in DSI studio, and tracts were generated by diffusion MRI fiber tracking (Figure 48).

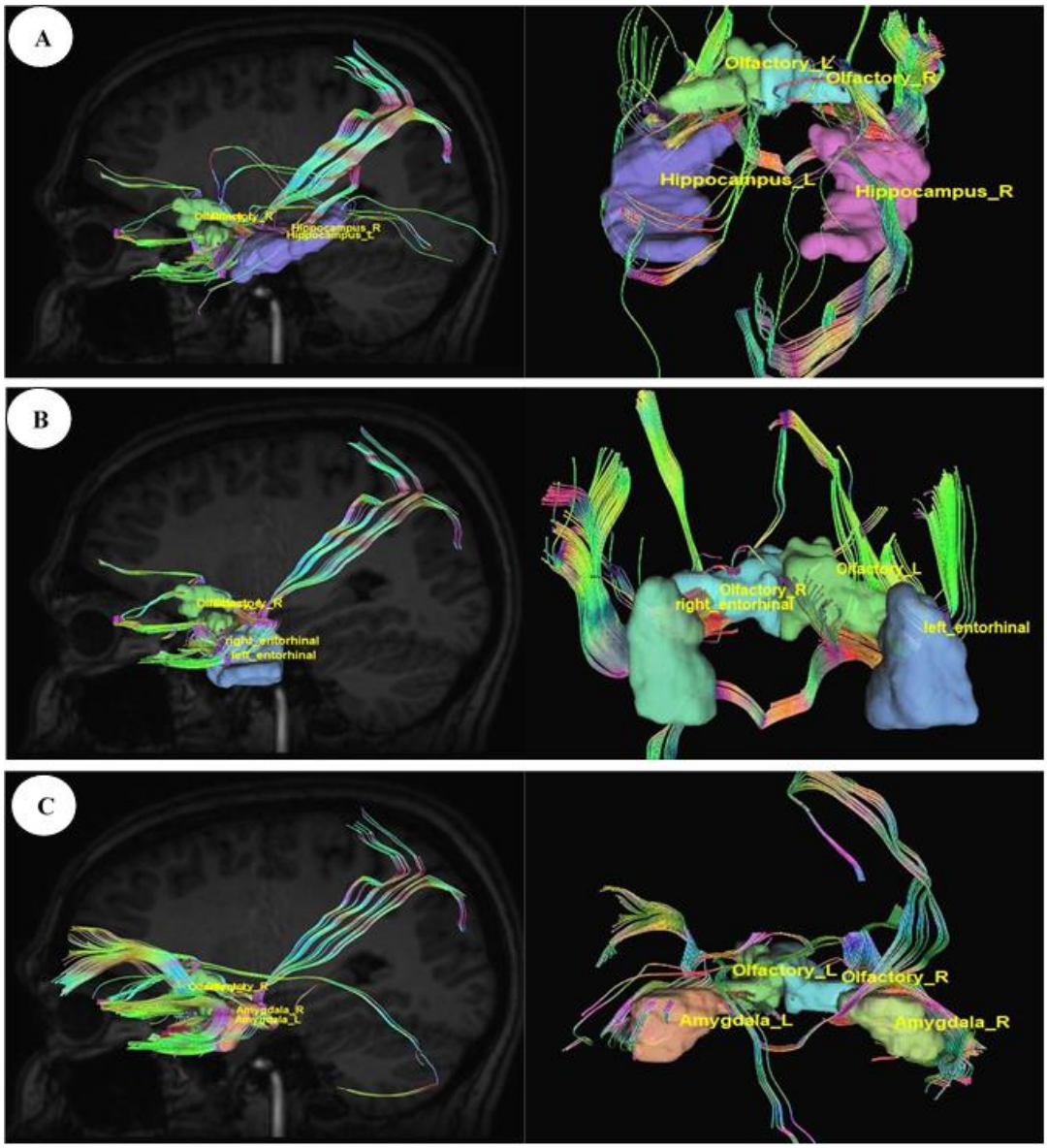

Figure 48: *Diffusion MRI fiber tracking connecting the olfactory nerve with (A) the hippocampus, (B) the entorhinal cortex, and (C) the amygdale.*

9.3.2 Docking Study

9.3.2.1 Binding Sites of ACE Receptor

Severe Acute Respiratory Syndrome Coronavirus 1 and 2 both utilize common receptor angiotensin-converting enzyme 2 (ACE2) for binding. We have studied the binding affinity of the tetracycline class of drugs toward the binding sites of the ACE-2 receptor, where the receptor-binding domain of SARS-COV attached. ACE inhibitors and angiotensin-receptor blockers are used globally to produce beneficial cardiorenal effects [178]. Several studies reported that using ACE inhibitors in patients with COVID19 can increase the severity by increasing the expression of ACE2 receptors, which are crucial for virus entry [179].

We have identified that the ACE 2 receptor has two different kinds of binding sites, Site A where the ACE inhibitors like MLN-4760, lisinopril drugs are bound (PDB ID: 1R4L) [180], and Site B is the virus-binding site (PDB ID:6M0J) [181] (Figure 49). The two binding sites of angiotensin-converting enzyme (ACE): Site A is the binding site for ACE inhibitors, which helps in preventing the conversion of Angiotensin I to Angiotensin II producing vasodilation, and Site B is the virus-binding site through which viral entry takes place. ACE inhibitors show less-binding affinity toward the virus binding site (Site-B), where the tetracycline class of drugs shows more negative values of binding energy, indicating the stability of the interaction.

Our study revealed that the standard ACE inhibitors had got less binding affinity toward the virus-binding site of the ACE 2 receptor. Docking scores for MLN-4760 and lisinopril are −2.62kcal/mol and −2.16 kcal/mol in the virus-binding site (Site B), respectively, whereas it is −8.11 kcal/mol and −8.15 kcal/mol, respectively, in the ACE inhibitor-binding site of ACE2 receptor (Table 10, Figure 50).

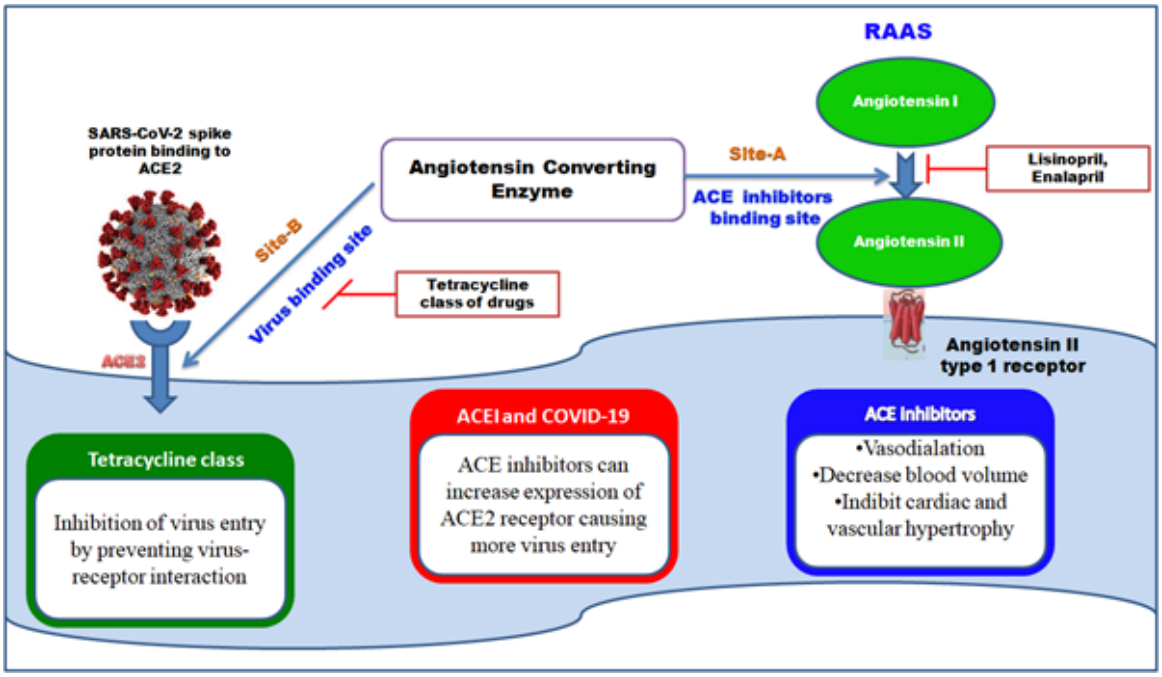

Figure 49: *The binding site of ACE inhibitors and SARS-COV2 spike protein.*

Table 10. The comparison of binding energy and inhibitory constant (Ki) value of ACE inhibitors against inhibitor bound human angiotensin converting enzyme-related carboxypeptidase (ACE2) (PDB ID: 1R4L) and SARS-CoV-2 spike receptor-binding domain bound to the ACE2 receptor (PDB ID: 6M0J).

Compounds	**Site A (PDB ID: 1R4L)**			**Site B (PDB ID: 6M0J)**		
	Total binding energy (kcal/mol)	**Calculated inhibitory constant (Ki-Molar)**	**Interacting amino acid residues**	**Total binding energy (kcal/mol)**	**Calculated inhibitory constant (Ki-Molar)**	**Interacting amino acid residues**
MLN-4760	-8.11	1.13×10^{-6}	Arg273 His345 Pro346 Thr371	-2.62	1.20×10^{-2}	Gln24
Lisinopril	-8.15	1.07×10^{-6}	Arg273 His345 Pro346 Thr371	-2.16	2.59×10^{-2}	Gln24

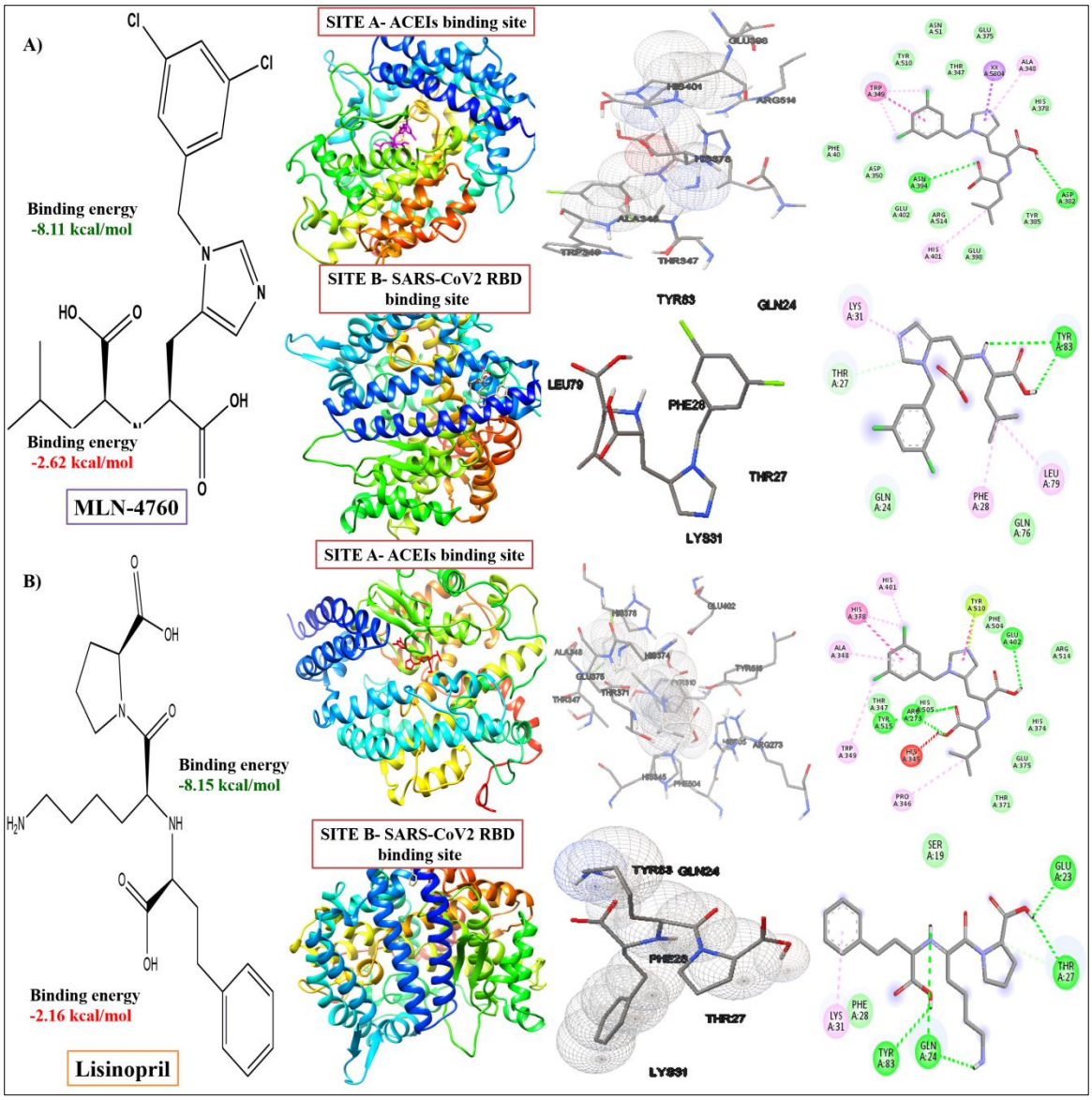

Figure 50: *Computed structural comparison, binding features, and the 2D interaction plot (visualization using UCSF Chimera, AutoDock and Biovia discovery studio) of MLN-4760 ((S,S)-2-{1-carboxy-2-[3-(3,5-dichlorobenzyl)-3H-imidazol4-yl]-ethylamino-4-methylpentanoic acid) (A) and lisinopril (B), with two binding sites of theACE-2 receptor (PDB ID: 1R4L and 6M0J, respectively).*

9.3.2.2 Interaction Between ACE2 Receptor and SARS-COV2

The critical interacting residues present in the ACE2 receptor, which displayed interaction with the SARS-COV2 spike receptor binding domain, were divided into three parts: N terminal, a middle portion, and C terminal. A network of hydrogen bonds formed between Gln498, Thr500, and Asn501 of the RBD with Tyr41, Gln42, Lys353, and Arg357 residues of ACE2 receptor, respectively. Lys417 and Tyr453 residues of the middle portion

of RBD interact with Asp30 and His34 of the ACE2 receptor, and, at the C terminal, Gln474 of RBD is H-bonded to Gln24 of ACE2, while Phe486 of RBD interacts with Met82 of ACE2 through vander Waals forces, respectively [181, 182] (Figure 51).

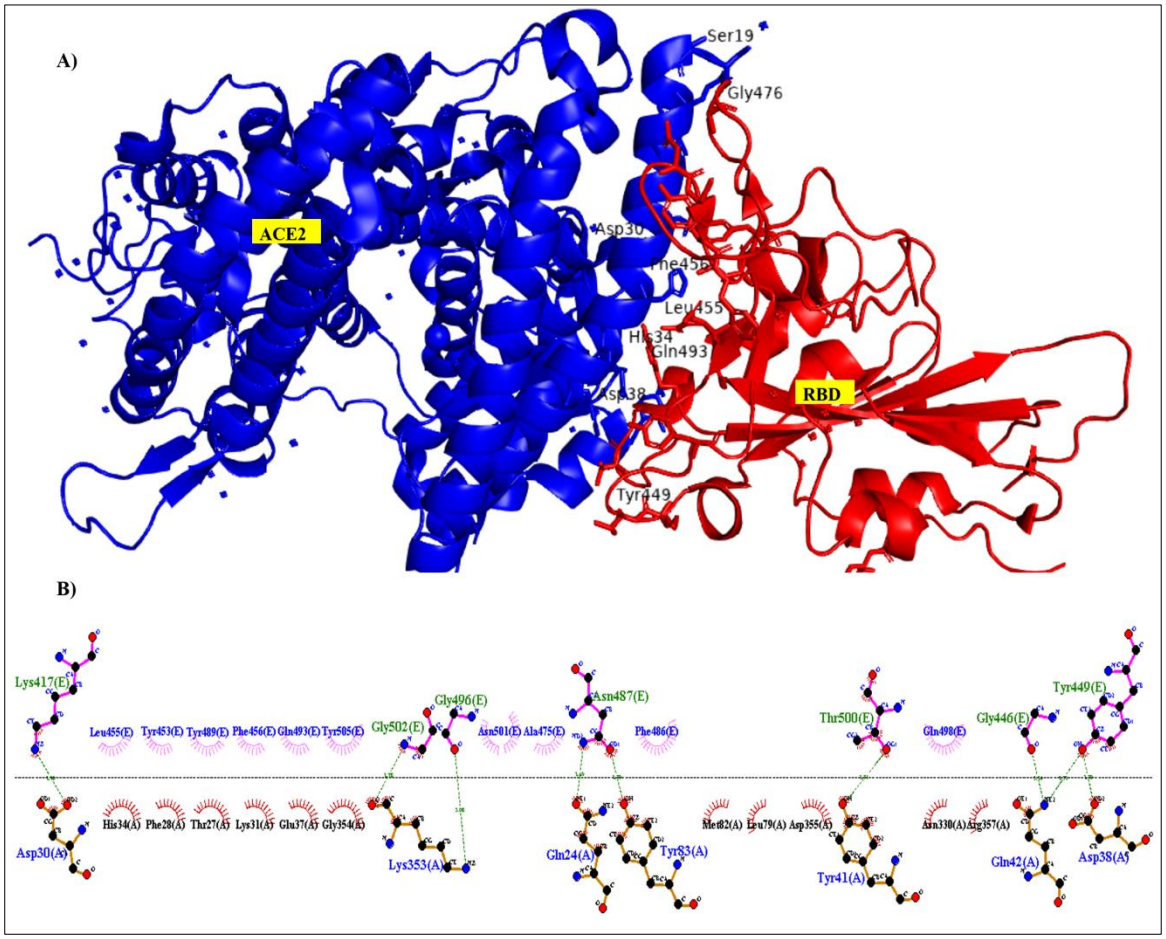

Figure 51: *Interacting amino acid residues between the Angiotensin-Converting Enzyme 2 (ACE2) receptor and SARS-COV2 Receptor Binding Domain (RBD) (A)and the 2D interaction plot (B), visualized using PyMol and LigPlus.*

9.3.2.3 Interaction Between ACE2 Receptor with Tetracycline Ligands and Phytochemicals

For the docking study, the grid was formed around the interacting residues of the ACE2 receptor, which were Tyr41,Gln42, Lys353, Arg357, Asp30, His34, Gln24, and Met82 [181]. The interaction of ligands with the receptor is shown in Figure 52, and the free energy of binding along with inhibition constant (Ki) is tabulated in Table 11. In our study, we have observed that, in comparison to the standard tetracycline class (Tetracycline,

Minocycline, and Doxycycline), phytochemical chlorogenic acid and the newer type of tetracycline-like fluorocycline (Ervacycline) show greater, and glycylcycline (Tigecycline) shows a comparable binding affinity toward the SARS-COV2 virus-binding site of the ACE2 receptor. There were several interactions among the receptor and ligands in which chlorogenic acid interacted with Ser373 and Trp436; minocycline interacted with Asp30 and His34; Naringenin interacted with Phe338 and Cys336; Tetracycline interacted with Gln24 and Met82, Doxycycline with Asp30, Tigecycline with His34, and Ervacycline with Gln24 amino acid residues among other interactions. The amino acid residues mentioned were the residues present in the SARS-COV2 spike receptor-binding-domain-attaching sites of the ACE2 receptor. However, podophyllotoxin showed lower binding affinity with less inhibition constant toward the ACE2 receptor.

Table 11. The increasing order of binding energy and inhibitory constant (Ki) value of phytochemicals, tetracycline class of antibiotics and ceftriaxone against with SARS-CoV-2 spike receptor-binding domain bound to the ACE2 receptor (PDB ID: 6M0J).

Compund	Total binding energy (kcal/mol)	VDW + H bond + desolv Energy (kcal/mol)	Calculated inhibitory constant (Ki- Molar)	Interacting amino acid residues
Chlorogenic acid	-9.02	-10.48	2.45×10^{-7}	Trp436 Ser373 Asn437 Phe342
Ervacycline	-8.23	-9.91	9.26×10^{-7}	Gln24 Gln76 Phe28 Glu76
Rolitetracycline	-7.30	-9.13	4.43×10^{-6}	Gln76 Thr27 Lys31 Leu79
Tigecycline	-7.28	-8.97	4.61×10^{-6}	His34 Asn33 Glu37 Phe390
Minocycline	-7.27	-8.46	4.67×10^{-6}	Asp30 His34 Pro389 Phe390
Naringenin	-7.07	-8.18	6.57×10^{-6}	Phe338 Cys336 Leu335 Leu368
Tetracycline	-6.94	-8.32	8.13×10^{-6}	Gln24 Tyr63 Met82 Leu79
Quercetin	-6.36	-8.09	21.95×10^{-6}	Cys336 Asp364
Doxycycline	-6.19	-6.87	29.19×10^{-6}	Asp30 Leu29 Pro389 Gln96
Podophyllotoxin	-5.70	-8.53	6.62×10^{-6}	Gly482 Cys480 Asn481 Pro479
Ceftriaxone	-4.05	-7.11	1.08×10-3	Gln24 Thr27 Lys31 Leu79

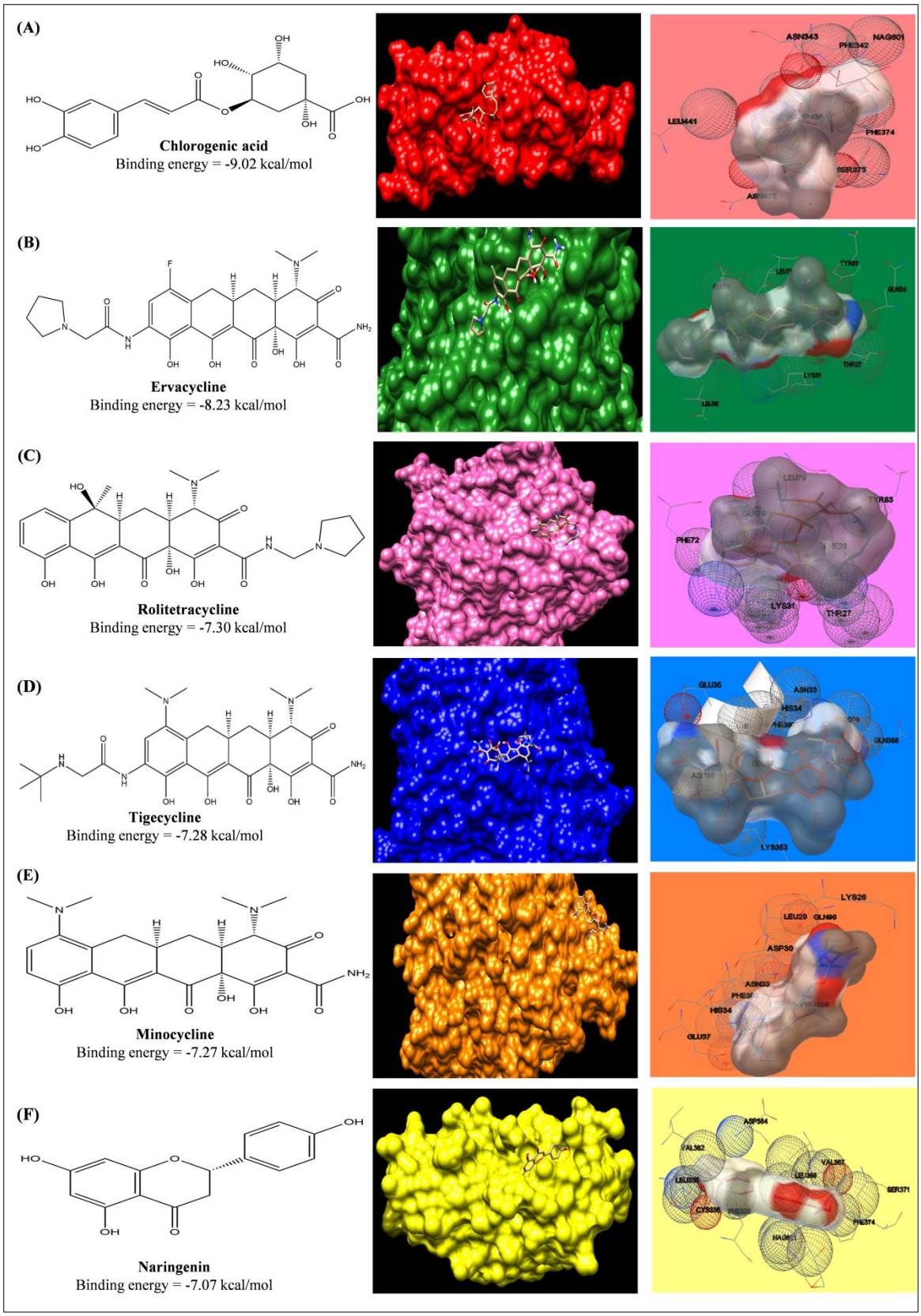

Figure 52: *Computed structural comparison and binding features (visualization using UCSF Chimera and AutoDock) of Chlorogenic acid (A), Ervacycline (B), Rolitetracycline (C), Tigecycline (D), Minocycline (E), and Naringenin (F) with Angiotensin-Converting Enzyme Receptor 2.*

9.3.2.4 Interaction Between SARS-COV2 Main Protease withTetracycline Ligands and Phytochemicals

In a similar fashion, grid was formed around COVID-19 main protease where its potent inhibitor N3 was bound. The interacting amino acid residues of the protease were His41,Cys145, Phe140, Gly143, Pro168, Glu166, Ser144, Met49, and Gln189 [183]. The interaction of ligands with the receptor is shown in Figure 53 and the free energy of binding along with inhibition constant (Ki) is tabulated in Table 12. Phytoconstituent chlorogenic acid, a newer class of antibiotics (Tigecycline and Ervacycline) and podophyllotoxin showed higher binding affinity toward SARS-COV2 main protease compared to standard tetracycline (Minocycline).

Table 12. The increasing order of binding energy and inhibitory constant (Ki) value of phytochemicals, tetracycline class of antibiotics and cephalosporin against COVID-19 main protease (6LU7).

Compound	Total binding energy (kcal/mol)	VDW + H bond + desolv Energy (kcal/mol)	Calculated inhibitory constant (Ki- Molar)	Interacting amino acid residues
Chlorogenic acid	-10.01	-11.50	45.96×10^{-7}	Gln189 Arg188 Met49 Phe140
Tigecycline	-8.85	-9.89	3.25×10^{-7}	His41 Gly143 His163 Gln189
Podophyllotoxin	-8.50	-11.92	5.91×10^{-7}	Glu166 Gln189 Met49 Asn142
Ervacycline	-8.09	-10.25	1.18×10^{-6}	His41 Gly143 Glu166 Pro168
Quercetin	-8.03	-9.73	1.30×10^{-6}	Glu166 Gln189
Minocycline	-7.82	-10.30	1.87×10^{-6}	HIS163 GLN189
Naringenin	-7.68	-8.71	2.37×10^{-6}	Gln192 Gln189 His41 Thr190
Ceftriaxone	-6.83	-10.53	9.09×10^{-6}	Gly143 Gln189 His164 His164

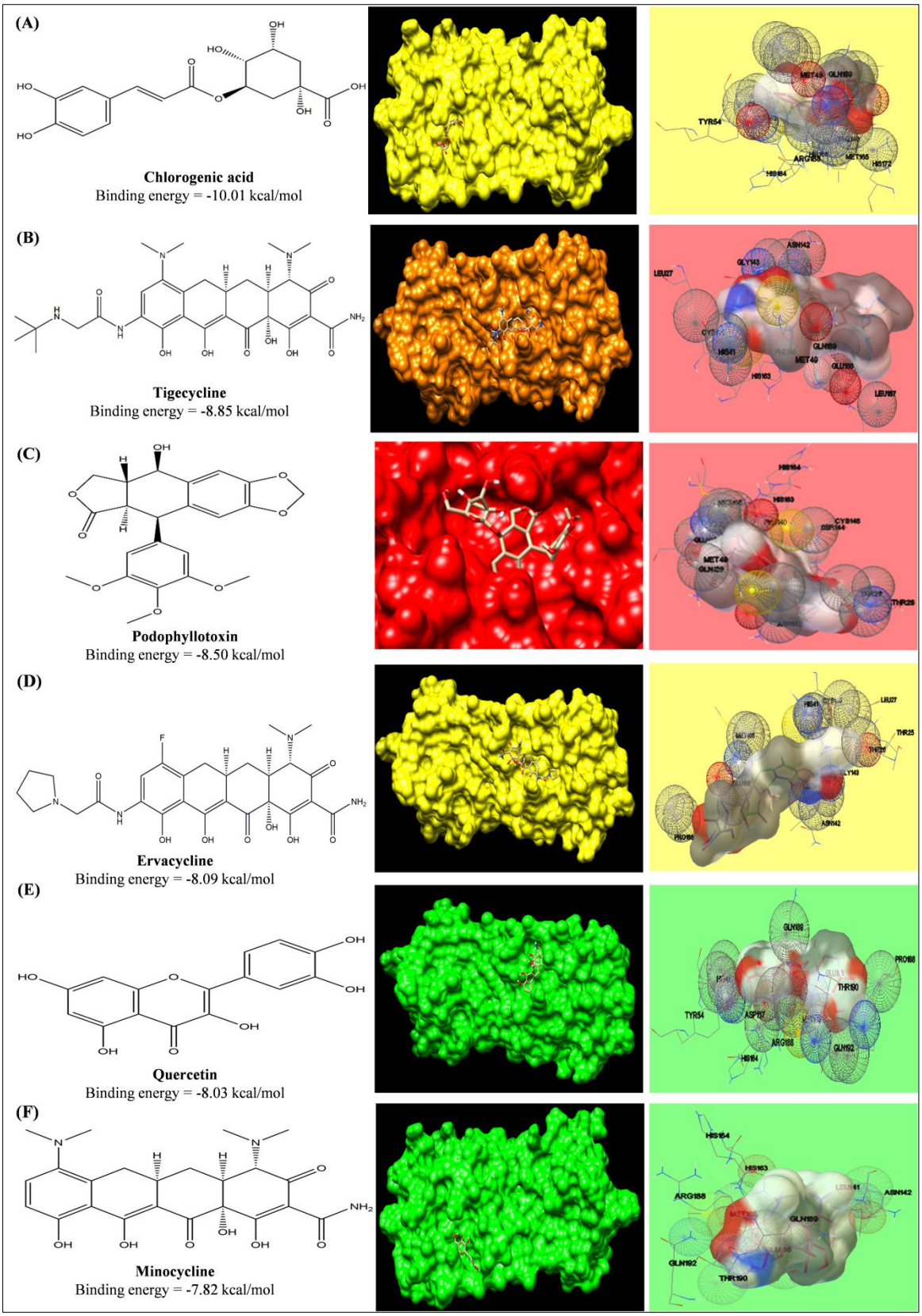

Figure 53: *Computed structural comparison and binding features (visualization using UCSF Chimera and AutoDock) of Chlorogenic acid (A), Tigecycline (B), Podophyllotoxin (C), Ervacycline (D), Quercetin (E), and Minocycline (F), with SARS-COV2 main protease. The lower the binding energy, the greater will be the binding affinity.*

9.3.3 Validation of Our Data

9.3.3.1 Docking Results with Japanese Encephalitis

A clinical trial of minocycline in treating Japanese encephalitis shows a better outcome [29]. To validate our data on whether the binding affinity of standard tetracyclines, cephalosporins, and phytochemicals toward the SARS-COV2 can be pharmacologically effective or not, we have compared the binding affinity of minocycline with COVID-19 main protease to the binding affinity of minocycline against NS3 helicase/nucleoside triphosphatase of Japanese encephalitis (J.E.), which possesses enzymatic activities of a serine protease, helicase, and nucleoside 5'-triphosphatase (NTP). In accordance with an earlier docking study done by Nath, M. et al., between minocycline and NS3 helicase/NTPase of J.E. virus, the docking score was around −115.024 kcal/mol calculated via iGEMDOCKv2.1 [184], which was approximately −7.82kcal/mol when calculated via AutoDock 1.5.6. In our study, we have found similar binding affinity of minocycline (−7.66kcal/mol) and ervacycline, with more negative values of binding free energy (−9.81 kcal/mol), with SARS-COV2 main protease indicating potential of these agents in treating COVID-19 (Figure 54). Moreover, we have compared the binding affinity of chlorogenic acid toward NS helicase of JE virus (−7.80 kcal/mol), which also revealed equivalent values (Table 13). Furthermore, the binding affinity of ceftriaxone (−6.76 kcal/mol) toward NS helicase of JE virus was comparable with other phytochemicals, such as podophyllotoxin (−6.47 kcal/mol), naringenin (−6.16 kcal/mol), and quercetin (−6.13 kcal/mol).

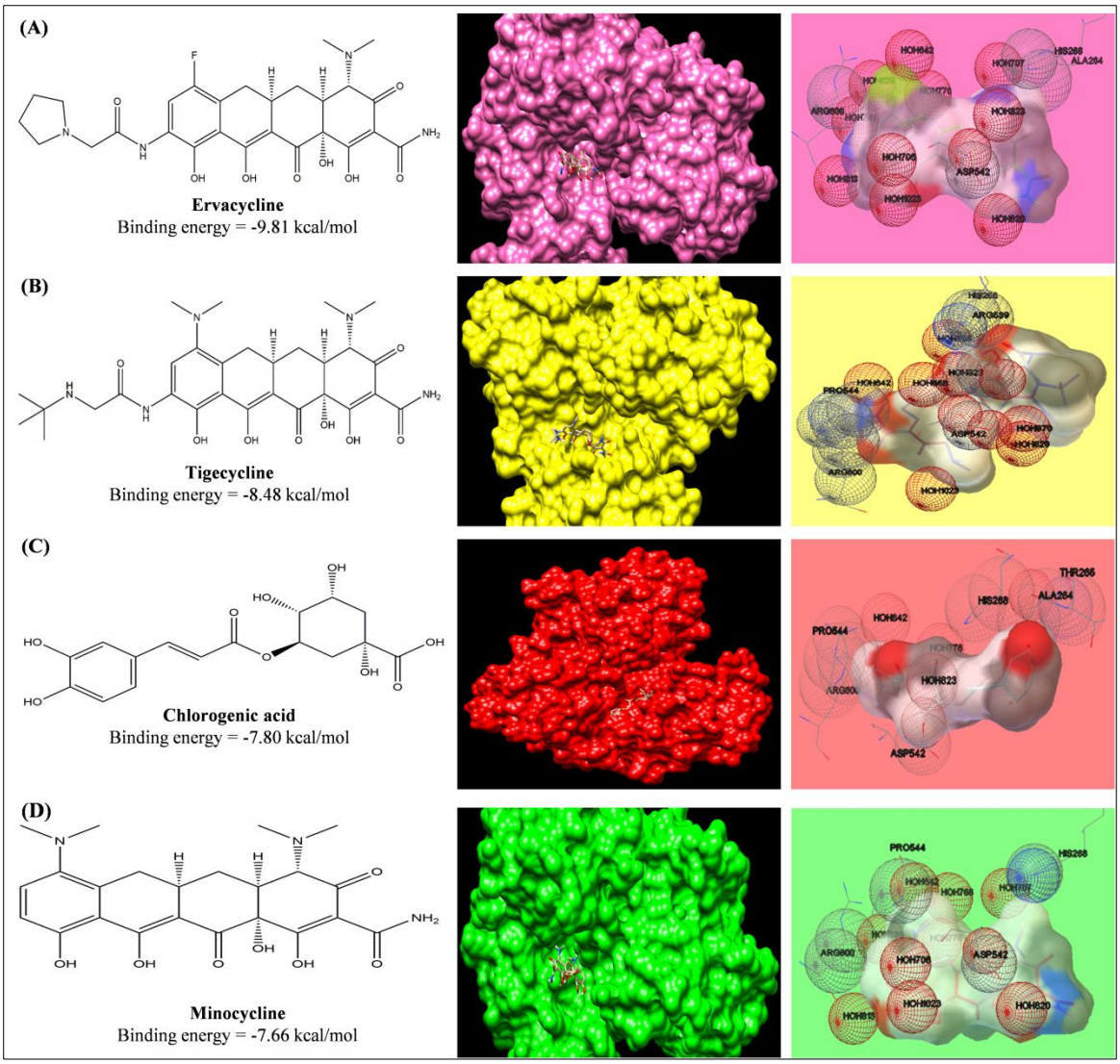

Figure 54: *Computed structural comparison and binding features (visualization using UCSF Chimera and AutoDock) of Ervacycline (A), Tigecycline (B), Chlorogenic acid (C), and Minocycline (D), with NS3 helicase/nucleoside triphosphatase of Japanese encephalitis.*

Table 13. *The increasing order of binding energy and inhibitory constant (Ki) value of phytochemicals, tetracycline class of antibiotics and cephalosporin against N.S. helicase/ nucleoside triphosphatase of Japanese encephalitis (PDB ID: 2Z83).*

Compound	Total binding energy (kcal/mol)	VDW + H bond + desolv Energy (kcal/mol)	Calculated inhibitory constant (Ki-Molar)	Interacting amino acid residues
Ervacycline	-9.81	-11.36	6.48×10^{-7}	Ala264 His266
Tigecycline	-8.48	-10.84	6.11×10^{-7}	Asp542 Pro544
Chlorogenic acid	-7.80	-9.07	1.91×10^{-6}	Asp542 Arg600
Minocycline	-7.66	-9.06	2.42×10^{-6}	Asp542 Arg600

9.3.3.2 Modeling with clinical trial findings

We simulate the model (1)-(3), taking data points from the Kaplan Meier Survival curves generated between Minocycline treated group and Ceftriaxone (relative placebo) treated group in randomized clinical trial of Minocycline in Acute Encephalitis Syndrome carried out by Kumar R et al.,[29].

From equation (4) we can write:

$$n\,(t) = {}^{n}C\,(t) + {}^{n}V\,(t) = {}^{n}C_0 \times e^{-\alpha t} + {}^{n}V_0 \times e^{-\beta t}$$

Analogously, we can write

$$R^{\%}_{both} = R^{\%}_{(cell\ wall)} * e^{-\alpha t} + R^{\%}_{(virus\ wall)} * e^{-\beta t}$$

Here the following symbols are used:

$R^{\%}_{(cell\ wall)}$ = Percentage of cell wall receptors occupied by drug

$R^{\%}_{(virus\ wall)}$ = Percentage of viral wall receptors occupied by drug

$e^{-\alpha t}$ = Number of cell wall receptors occupied by drug decays with time, as cells learns or develops to efflux or chemotolerance.

$e^{-\beta t}$= Number of virus wall receptors occupied by drug decays with time in first week (drug given continuously), as virus learns or develops to efflux or chemotolerance.

After simulating the equation, we have obtained the values of percentage of receptor occupancy, α and β (Figure 55).

Hence, we obtain:

(i) Interaction of Minocycline with receptors

$$R^{\%}_{both} = 0.7044126 * exp^{(-0.0003975881 * t)} + 0.2955874 * exp^{(-0.3274611 * t)}$$

(ii) Interaction of Ceftriaxone (relative placebo) with receptors

$$R^{\%}_{both} = 0.6558881 * exp^{(-0.001120362 * t)} + 0.3441119 * exp^{(-0.2023223 * t)}$$

Comparing these two equations, it can be revealed that ceftriaxone shows predominantly virucidal activity with rapid decaying (α = 0.001120362) compared to minocycline which shows both virucidal (α = 0.0003975881) as well as virostatic activity (β = 0.3274611) with small values exhibiting slow decay with long term effects.

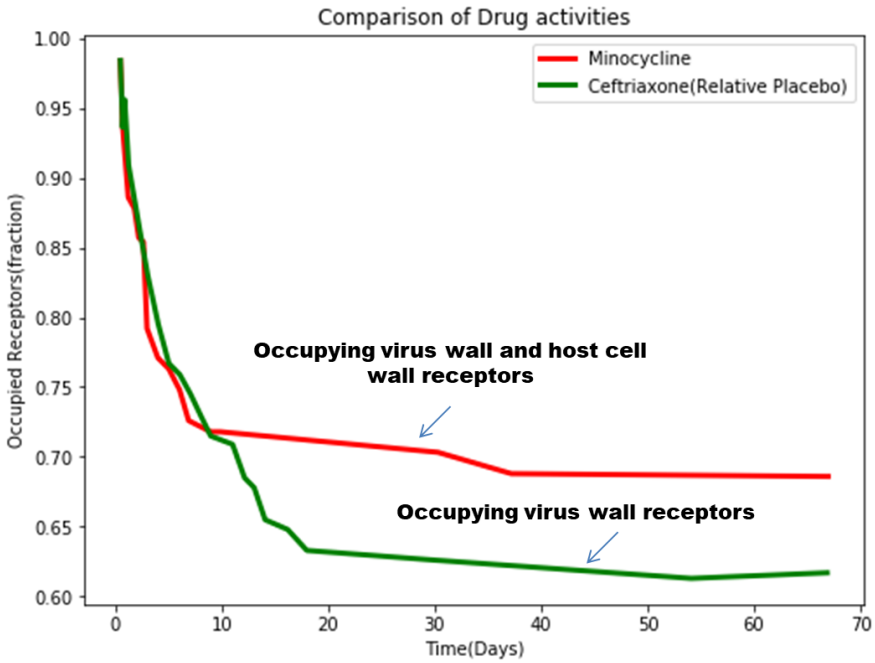

Figure 55: *The simulated mathematical model of drug activities toward receptors based on the clinical trial study.*

9.3.4 Network Pharmacology Analysis

9.3.4.1 Targets Prediction Results

In this study, two categories of targets (Targets related to SARS-COV2, JE virus, and targets related to phytochemicals, standard drugs) were retrieved from different public databases (Table 14). According to UniProt, GeneCard, and NCBI databases, a total of 248 targets for SARS-COV2 and 346 targets for the JE viruswere found, from which the common targets with standard drugs and photochemical were identified by performing a Venndiagram analysis. These common targets were included for further studies.

Table 14: Total number of retrieved targets from different databases.

Category	Database	Number	Total number of unique targets	Number of common targets with disease	CytoNCA Predicted top 10 genes
Disease targets					
COVID19	UniProt GeneCard NCBI	27 239 8	248		
JE	UniProt GeneCard NCBI	10 344 9	346		
Drug targets					
Ceftriaxone	GeneCard DrugBank	40 88	88	24	IFNG, HLA-DRA, CXCL8, IL6, IL10RA, CD4, IL1R1, IL6ST, IL1B, TNF
Chlorogenic acid	GeneCard DrugBank	25 43	68	11	JUN, NFE2L2, MAFK, MTOR, NFE2, MAFG, HIF1A, NOS3, IL1B, ATP2B1
Minocycline	GeneCard DrugBank	91 46	136	39	CCL5, CXCL8, CCL2, STAT1, IFNG, CCL18, CXCL9, CXCL10, CCR5, CCL4
Naringenin	GeneCard DrugBank	49 48	97	18	TP53, STAT3, FAS, AKT1, STAT1, JUN, TNFRSF1A, FADD, CREBBP, FASLG

Podophyllotoxin	GeneCard DrugBank	44 48	90	23	STAT1, IRF2, IRF1, STAT3, IFNG, ITGB2, ICAM1, JUN, IRF9, IRF3
Quercetin	GeneCard DrugBank	183 48	226	79	JUN, CXCL8, STAT1, IFNG, CCL2, STAT3, IRF1, CCL5, IL6, CXCL1

9.3.4.2 Gene–Gene Interaction Analysis

A Cytoscape plugin, GeneMania, was used to construct the gene-gene interaction network of targets of individual therapeutic agents (Figure 56). Circular nodes denoted genes, and colored edges presented their different correlations. Larger circles denoted that these genes were most correlated too their genes in this network. For detailed information of all the gene-gene interactions of individual agents, refer to Figures 57–61. Furthermore, topological parameters, Betweenness Centrality, Degree Centrality, and Closeness Centrality of each node, were observed. Degree Centrality is the measure of direct connections of a node in the network, and a higher degree indicates the high impact of thatnode. Based on the highest degree score, we selected the top10 nodes of the network.

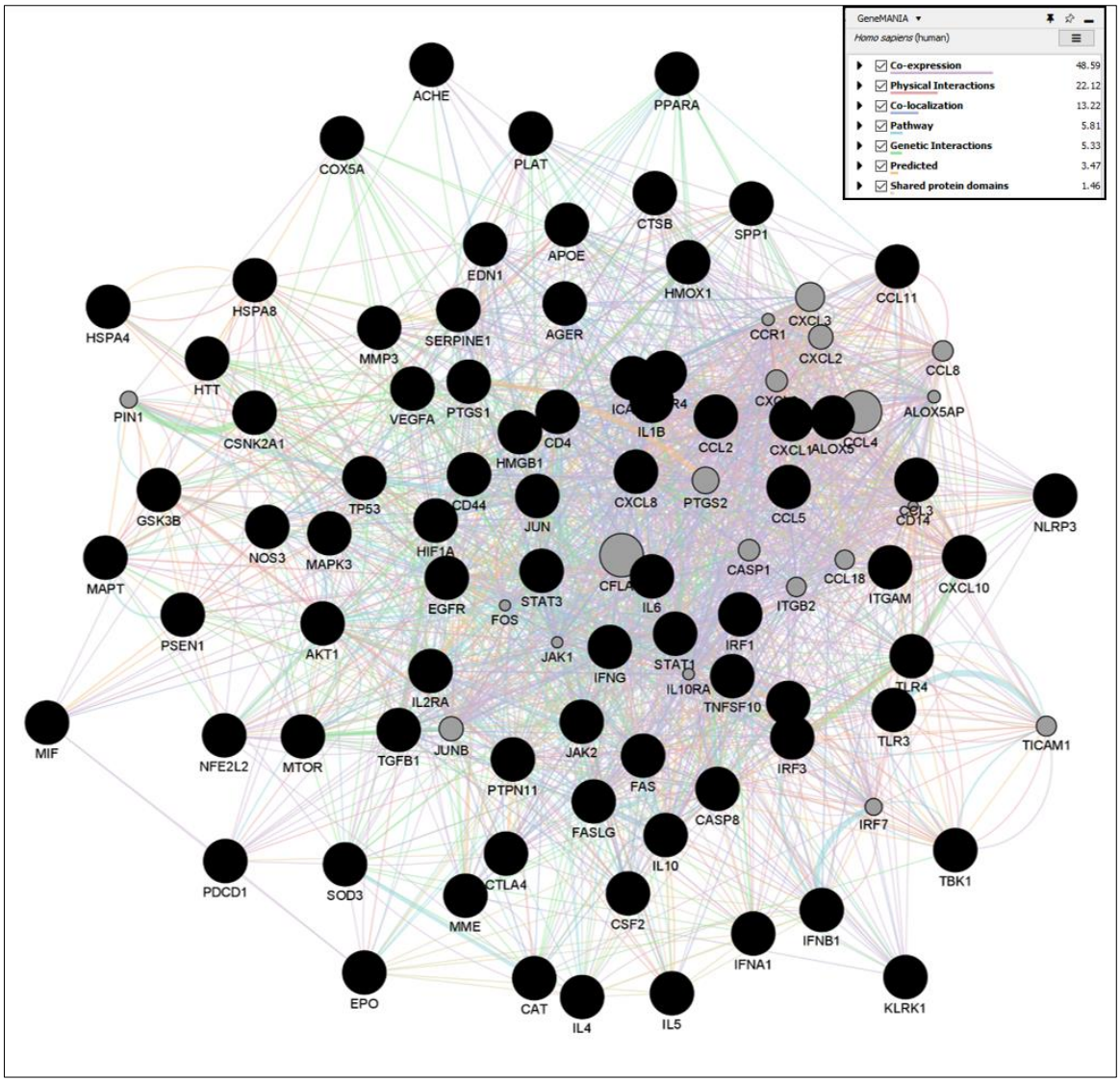

Figure 56: *GeneMANIA networks showing the gene-gene interaction results of Quercetin targets. Network displays the strength of interaction (edge thickness), type of interaction (colors), many edges in between nodes, and the score (size of node).*

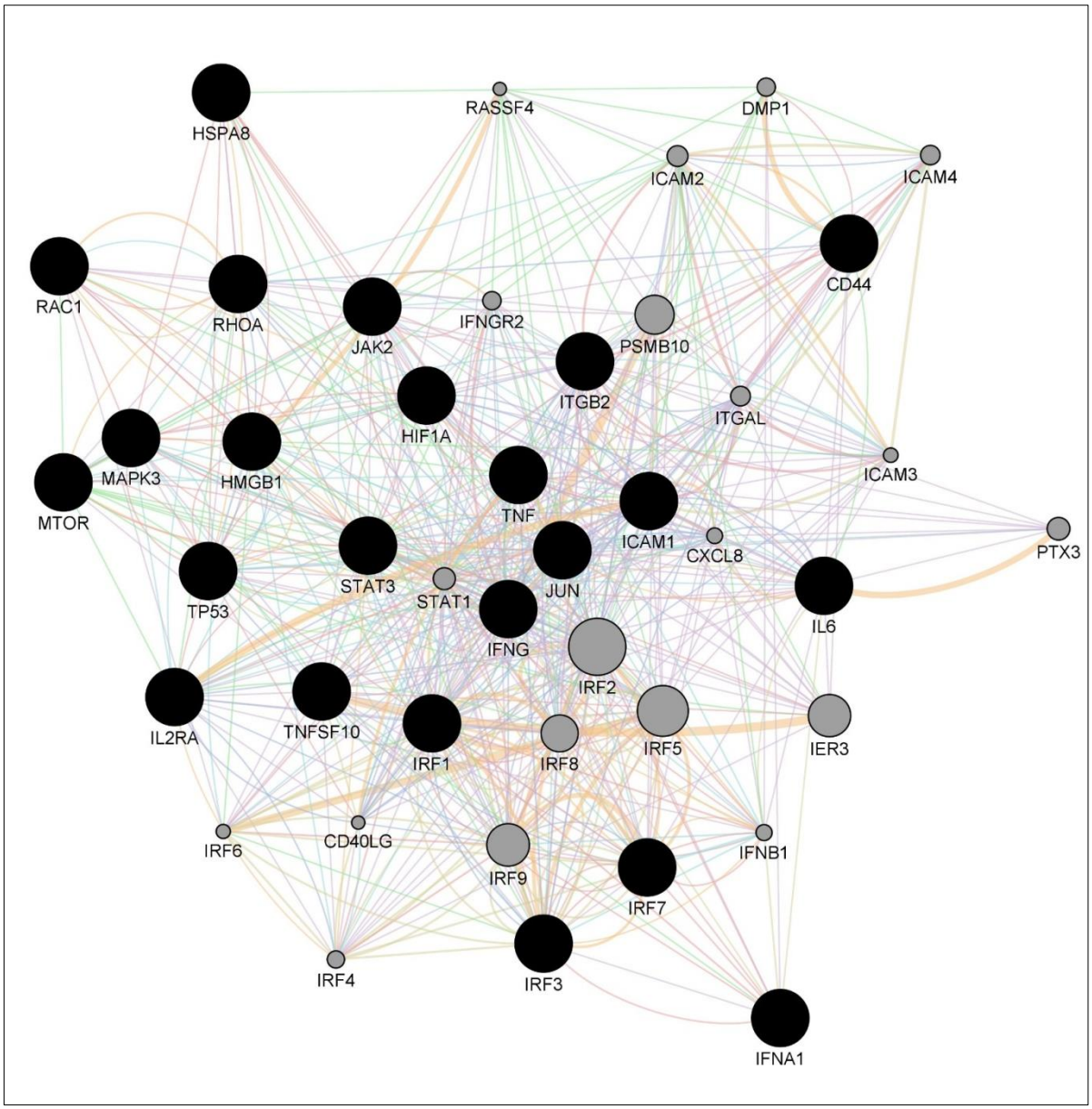

Figure 57: *GeneMANIA networks showing the gene-gene interaction results of Ceftriaxone targets. Network displays the strength of interaction (edge thickness), type of interaction (colors), many edges in between nodes, and score (size of node).*

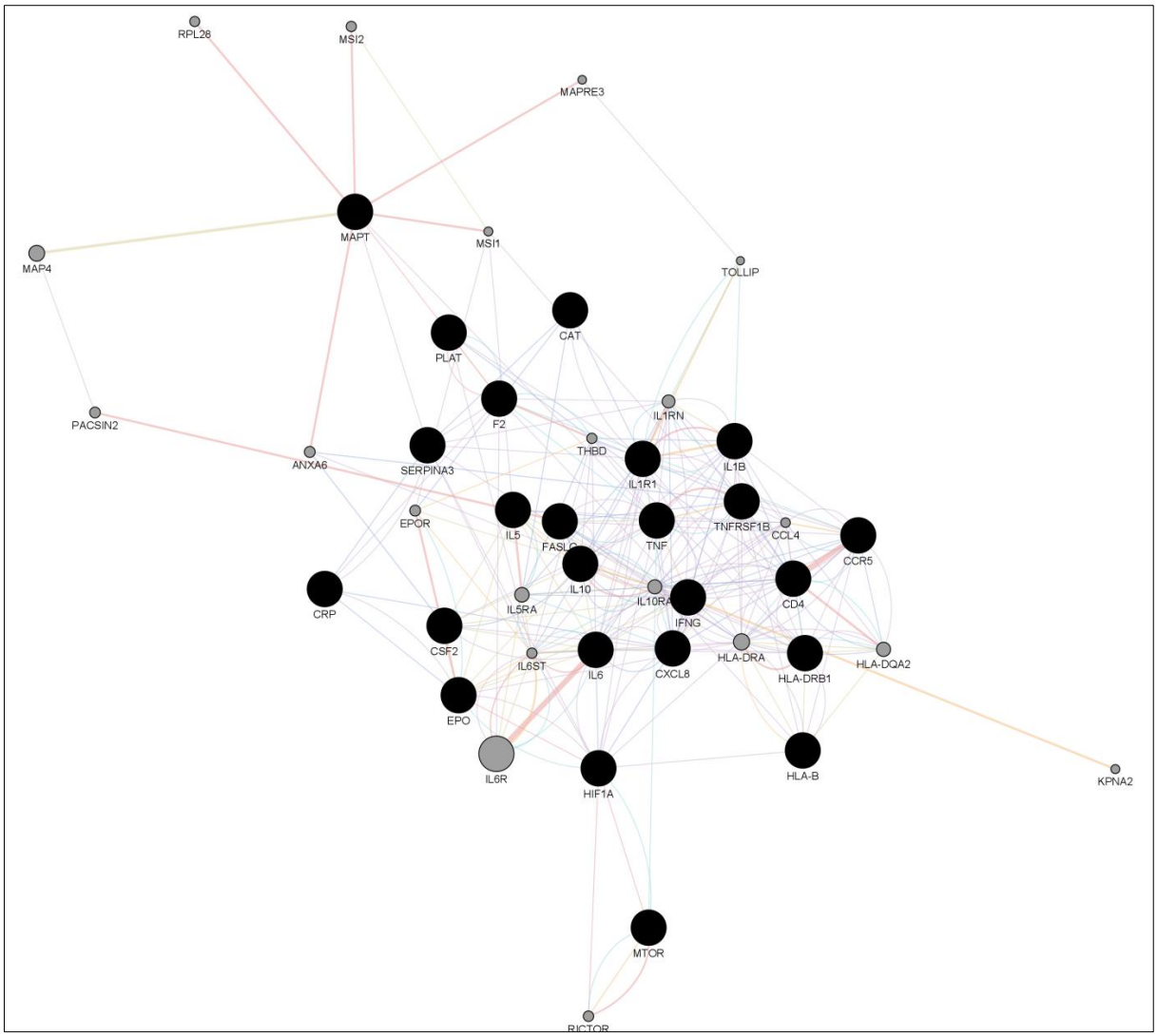

Figure 58: *GeneMANIA networks showing the gene-gene interaction results of Minocycline targets. Network displays the strength of interaction (edge thickness), type of interaction (colors), many edges in between nodes, and score (size of node).*

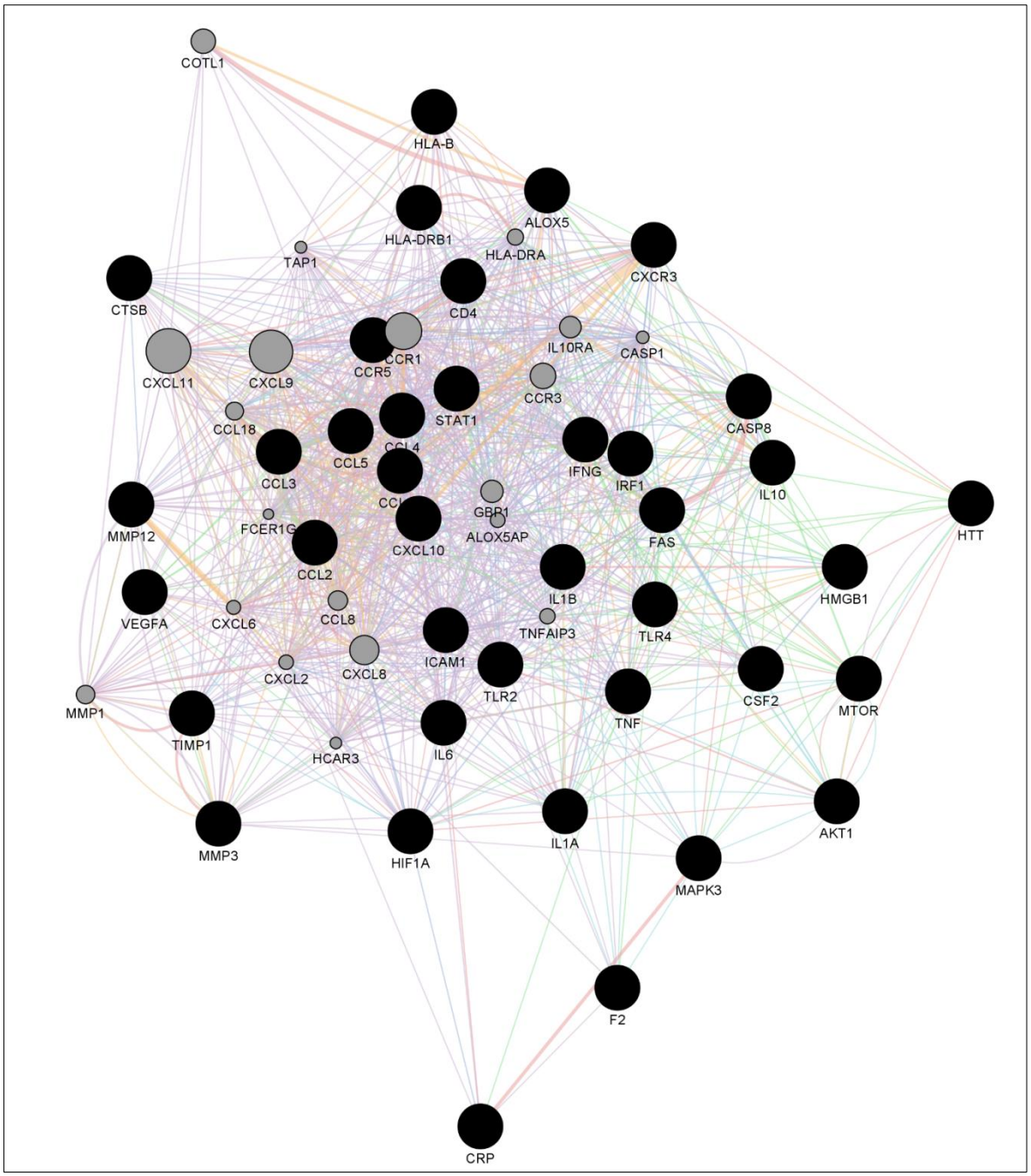

Figure 59: *GeneMANIA networks showing the gene-gene interaction results of Chlorogenicacidtargets. Network displays the strength of interaction (edge thickness), type of interaction (colors), many edges in between nodes, and score (size of node).*

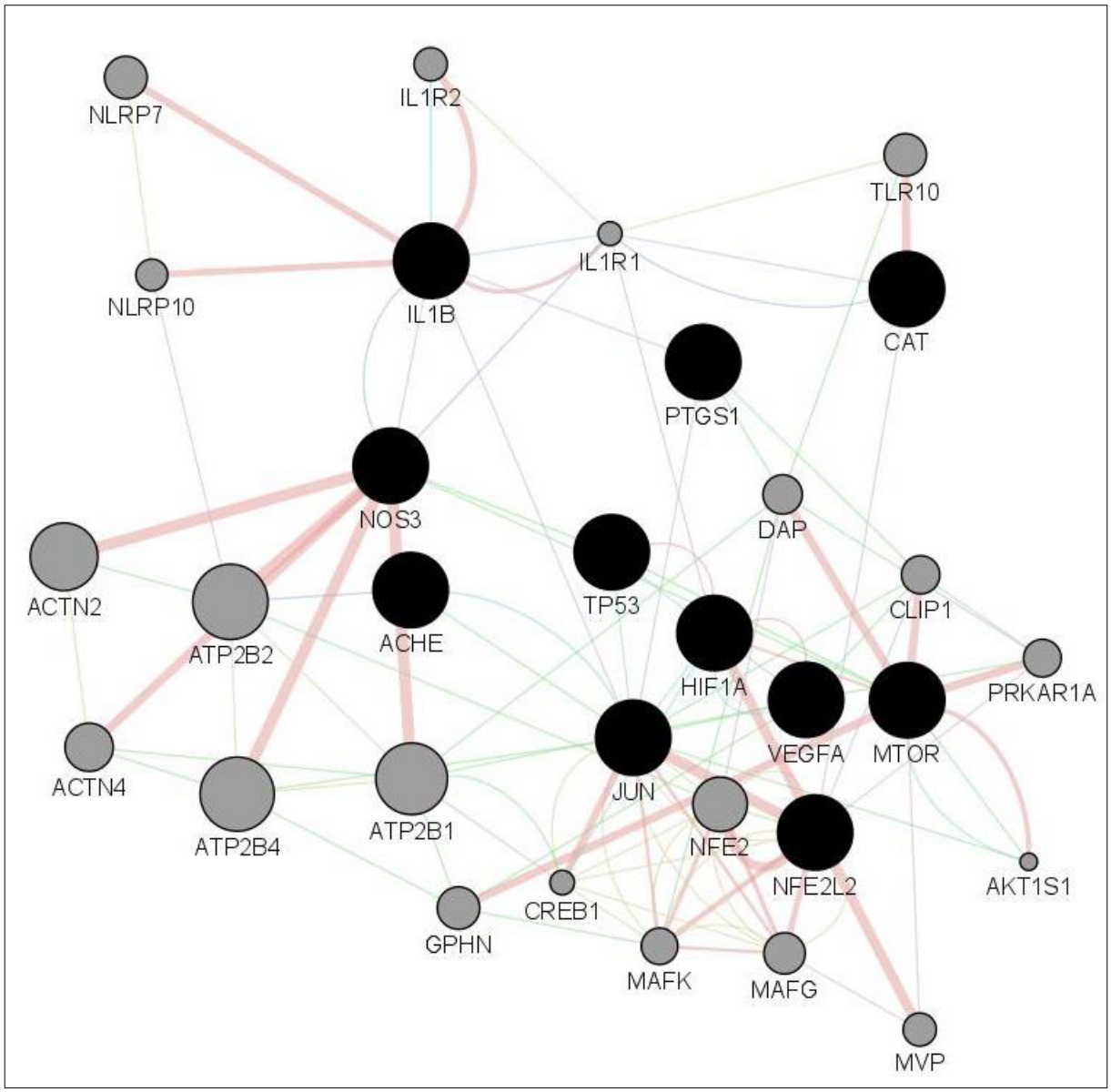

Figure 60: *GeneMANIA networks showing the gene-gene interaction results of Naringenintargets. Network displays the strength of interaction (edge thickness), type of interaction (colors), many edges in between nodes, and score (size of node).*

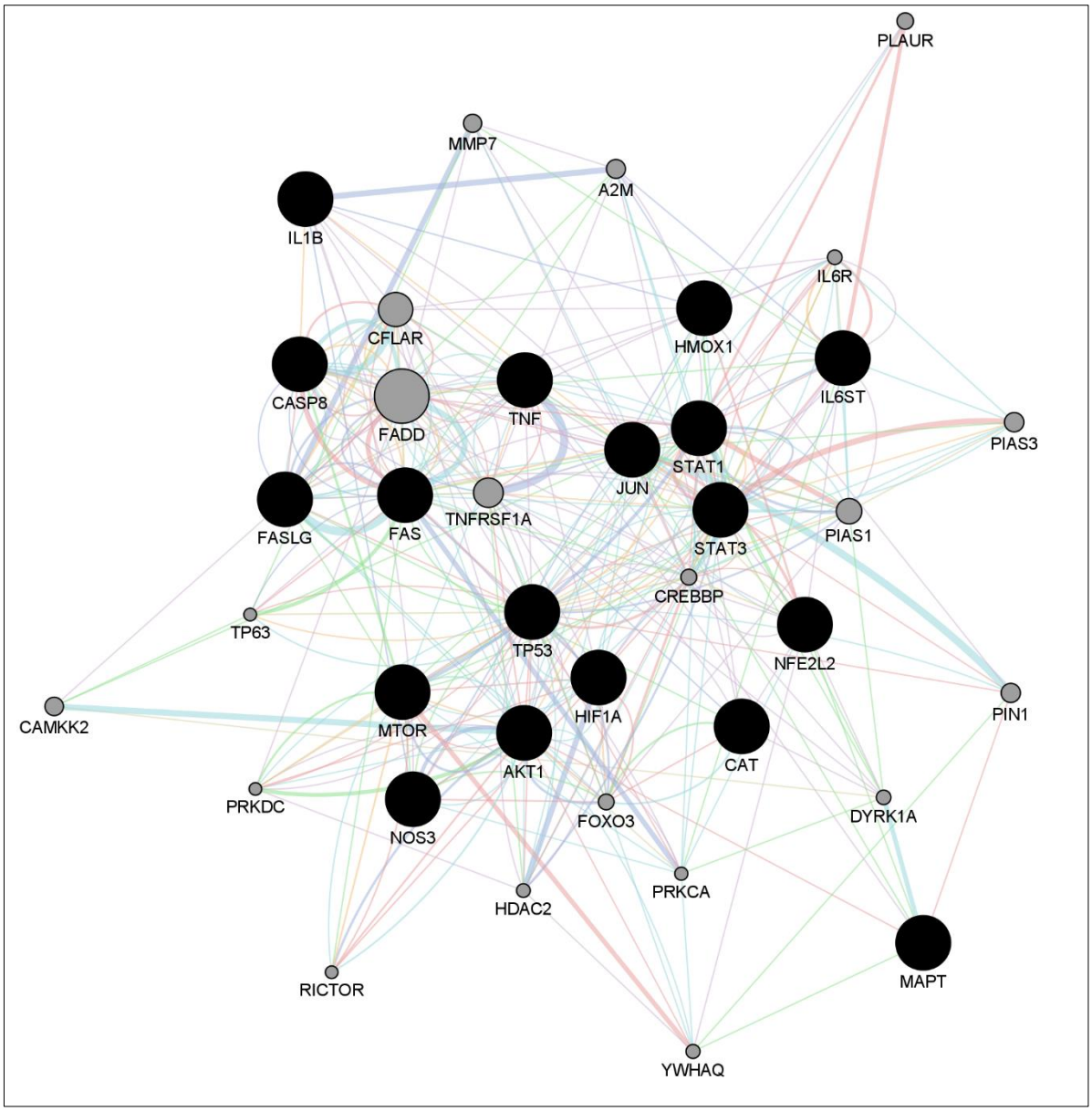

Figure 61: *GeneMANIA networks showing the gene-gene interaction results of Podophyllotoxin targets. Network displays the strength of interaction (edge thickness), type of interaction (colors), many edges in between nodes, and score (size of node).*

9.3.4.3 Gene Ontology and KEGG Enrichment Analysis for Targets

We have used PANTHER to obtain several Biological Processes (BP), Molecular Functions (MF), Cellular components (CC), Protein class, and pathways for ten key targets (Table 14) predicted in CytoNCA. In the case of BP, targets were enriched in different biological regulations, cellular processes, immunesystem processes, response to stimulus, and signaling. For CC, targets were enriched in the cellular, anatomical entity, intracellular, and protein-containing complex. In the case of MF, the targets were involved in binding, molecular function regulator, and molecular transducer activity. The targets were observed to be enriched in different protein classes like a defense/immunity protein, a intercellular signal molecule, and a transmembrane signal receptor. Pathways analysis of targets was enriched in Angiogenesis, B cell activation, Hypoxia response via HIF activation, Inflammation mediated by the chemokine and cytokine signalling pathway, the Interleukin signaling pathway, the JAK/STAT signaling pathway, T cell activation, and the Toll receptor signaling pathway. For more detailed resultsof all the categories, refer to appendix (Table S4-S9). Inflammation mediated by chemokine and cytokine signaling pathways was the highest intensity in the gene ontology analysis, which substantiates that all the therapeutic agents targeted the cytostorm-mediated neuroinflammation during CNS infection. Moreover, the role ofthose critical genes in COVID-19 infection was also determined from the KEGG pathway (map05171) of Coronavirus disease (Figure 62).

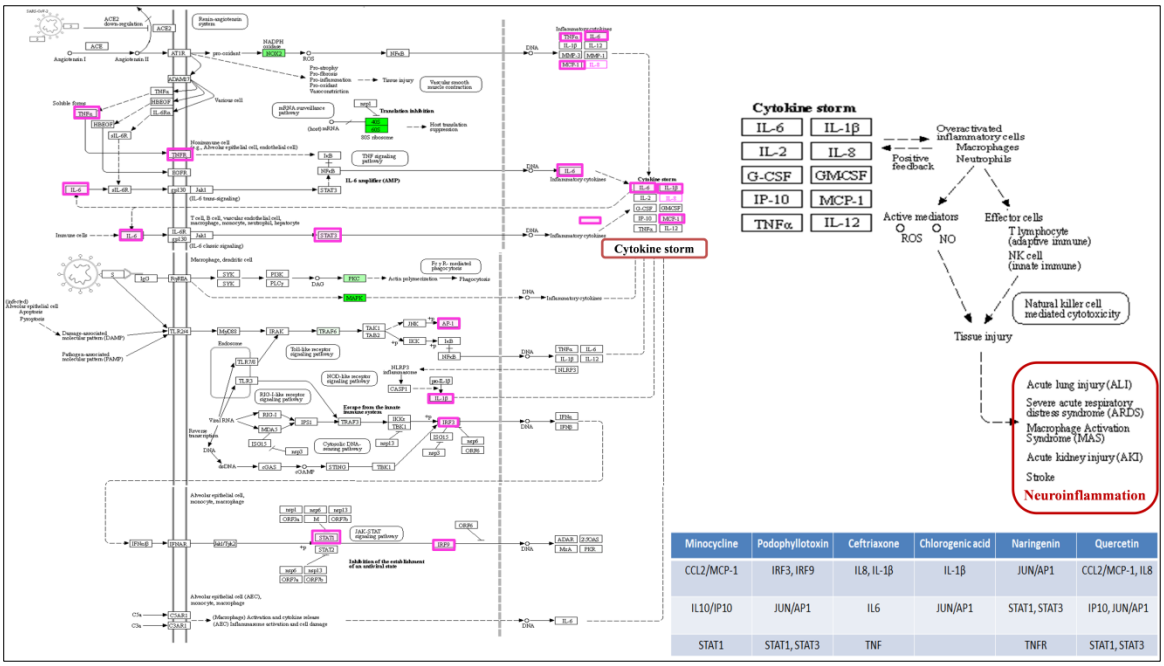

Minocycline	Podophyllotoxin	Ceftriaxone	Chlorogenic acid	Naringenin	Quercetin
CCL2/MCP-1	IRF3, IRF9	IL8, IL-1β	IL-1β	JUN/AP1	CCL2/MCP-1, IL8
IL10/IP10	JUN/AP1	IL6	JUN/AP1	STAT1, STAT3	IP10, JUN/AP1
STAT1	STAT1, STAT3	TNF		TNFR	STAT1, STAT3

Figure 62: *The KEGG pathway of Coronavirus Disease. The critical genes identified with CytoNCA are highlighted, and their role in cytokine storm-mediated neuroinflammation is depicted*

9.4 Discussion

The current epidemic of positive-sense single-stranded RNA virus produces some of the most lethal public health emergencies worldwide, e.g., MERS, SARS-1, COVID19, and Japanese Encephalitis. These viruses induce pan-systemic infection, and the death of patients occurs due to cytotoxic shock syndrome and central cardiorespiratory failure, i.e., dysfunction of theneural cardiorespiratory centre in the medulla oblongata and pons. These viruses are also neurotropic, and we delineate that they infect the respiratory centre of the brain (medulla) through anterograde transmission from nasal olfactory or pharyngeal cranial nerves and through retrograde transmission from the lung epithelium via the vagus nerve. Our findings were corroborated by other multiple studies where there were hyper-intense MRI signal changes in pons [185] in patients with COVID19, while penetration of SARS-COV2 through olfactory mucosa to medulla oblongata was also reported [186].

Some anti-viral pharmacological agents act by two mechanisms (i) virucidal activity: the agent directly damagesthe virus coat or its RNA [drug-virus receptor

interaction], and (ii) virustatic activity: the agent binds on the host cell receptor through which the virus enters, thus preventing virus entry into the host cell (Drug-Cell receptor interaction).

Additionally, we have developed a systems-biology-based double-hit mathematical bi-exponential model, which integrates these two aspects (virucidal and virustatic effects), and we validate this model by clinical findings of patient survival curves under antiviral treatment. This systems biology model furnishes a quantitative-clinical framework of action of phytochemicals and secondary metabolites on virus and host cells. Furthermore, multiple drugs can be given to modify the processes of cytotoxic shock syndrome. We have shown how phytochemicals and secondary metabolites can be explored for a meaningful therapeutic approach to such CNS infections.

In the present study, we have identified the nerve fiber tracts that enable the connection between gustatory nerves and the olfactory nerve with the respiratory center and limbic system, respectively these connections enable the centripetal spread of the virus from peripheral neural epithelium to thebrain, thus predisposing to central cardiorespiratory failure inthe brainstem region. Afterward, we have shown the binding affinity of the tetracycline drugs, the cephalosporins (ceftriaxone) and phytochemicals, with the Angiotensin-Converting EnzymeReceptor 2, which is the binding site for the SARS-COV2 spike (S) receptor-binding domain, as well as for COVID19 virus main protease that takes part in viral replication and transcription.

In our study, we evaluated the efficacy of phytochemicalsalong with secondary metabolites (as antibiotics) againstviral infection-mediated CNS inflammation. From the Docking studies, we have identified that the phytochemical, chlorogenic acid, as well as the newer class of tetracycline, ervacycline (a fluorocycline), showed more binding affinity

compared to the standard tetracyclines, as minocycline, or doxycycline, toward the SARS-COV2 receptor-binding site ofthe ACE2 receptor.

Furthermore, a phytochemical spectrum, as chlorogenicacid, podophyllotoxin, and quercetin, interacts with Gln189, Met49, Phe140, Glu166, Asn142 residues, which revealedthe robust binding affinity of these phytochemicals toward SARS-COV2 main protease, and is comparable with a newerclass of tetracyclines, namely, tigecycline and ervacycline. Furthermore, naringenin and quercetin bind with Cys336 residue, and podophyllotoxin binds with Cys480 residue of the receptor-binding domain; these cysteine residues stabilize the domain. Although binding affinity reveals that chlorogenic acid, ervacycline, and tigecycline were promising targets, the standard drug minocycline and tetracycline show more common interactions with SARS-COV2 spike protein against the ACE2 receptor. Moreover, we delineate that minocycline binds with the Asp30 and His34 amino acid residues in the SARS-COV2 spike protein, while tetracycline binds with the Gln24 and Met82 residues in that spike protein. However, ceftriaxone showed less binding affinity toward the host receptor and more toward COVID-19 protease, demarcating its predominant virucidal and less virustatic activity.

Considerable evidence indicates the therapeutic efficacy of minocycline in treating several viral infections like JapaneseEncephalitis, West Nile virus, Human ImmunodeficiencyVirus, Rabies, and Reovirus [187-189]. The anti-inflammatory and neuroprotective role of this broad-spectrum antibiotic was found to be effective in combating these neuroinvasive viruses. Independent of its antibiotic mechanism, minocycline can inhibit toxic microglia (M1) and activate neuroprotective microglia (M2), which leads to suppression of NF-kb activity, consequently preventing the production of pro-inflammatory cytokines, these are responsible for extreme acute respiratory distress symptom in patients with COVID19 [190, 191]. Our network pharmacology analysis

revealed that minocycline could target the pro-inflammatory chemokines (CCL2) and cytokines, whose abrupt increaseis referred to as cytokine storms [192]. Furthermore, it was reported that minocycline regulates endogenous matrix metalloprotease (the MMP-2 and 9 pathway) [193], whereas murine coronavirus utilizes host zinc metalloproteases for entry, survival, and cell-cell fusion [194, 195].

In addition to synthetic antibiotics, we observed that some phytochemicals substantially possess equivalent potency of antibiotics reported in alleviating CNS infection. To compare, Ding Y et al. reported the antiviral potential of chlorogenic acid against the influenza virus [196], and the acid has also beta-lactamase inhibitory potency, which is comparable with standard cephalosporins [160]. Several reports suggested that chlorogenic acid has shown therapeutic efficacy in SARS-COV2 infection by modulating inflammatory responses [197]. To corroborate, our gene ontology analysis identified that chlorogenic acid could target neuroinflammation mediated by chemokine and cytokine signaling pathways. It has also been revealed that phytochemicals, as naringenin [161] and quercetin [198], also show antiviral and anti-inflammatory properties, like reducing viral replication and interacting with downstream signaling molecules of Toll like receptors (TLRs), as well as the JAK-STAT pathway. Furthermore, we inferred that podophyllotoxin has equivalent therapeutic potential as teracyclines [158], besides proving to be effective against cytokine storm in patients with COVID-19 [199]. Our findings suggest that podophyllotoxin could also target IFN-regulatory Factors 3 and 9, which are crucial in SARS-COV-mediated evasion of host innate immune response [200].

9.5 Conclusion

The crucial findings of our investigations suggest that phytochemicals and secondary metabolites have both virostatic and virucidal mechanisms to ameliorate CNS infection. To exemplify, phytochemicals as podophyllotoxin and quercetin manifested a greater binding

affinity toward the virus protease, suggesting their strong virucidal mode of action. Moreover, our network pharmacology approach substantiates the possible mechanism through which the phytochemicals and secondary metabolites have seminal possibilities in alleviating CNS infection. A noteworthy finding is that ascending viral infection, migrating retrogradely via nerve fibers, can induce respiratory failure by affecting the midbrain, and hence phytochemicals, which have a satisfactory CNS permeation profile, may offer a novel therapeutic avenue to resistant neurotropic viral infections.